1π resonance of CO on Pt(111) studied by angle-resolved ultraviolet photoelectron spectroscopy

Thorben Haarlammert,[1,*] Alexander Victorovich Golovin,[2] and Helmut Zacharias[1]
[1]*Physikalisches Institut, Westfälische Wilhelms-Universität, D-48149 Münster, Germany*
[2]*Institute of Physics, St Petersburg State University, 198504 St. Petersburg, Russia*
(Received 8 November 2010; published 31 March 2011)

The photoemission cross section of the $1\pi^{-1}$ state shows a significant resonance at a photon energy of $h\nu = 33$ eV, which so far has not been observed in gas-phase measurements nor on surfaces of other transition metals. The occupied electronic states of CO adsorbed on the platinum (111) surface are investigated theoretically and experimentally. Photoelectron angular distributions at various photon energies across this particular resonance are recorded to achieve further information on the nature of the electronic states involved. These photoelectron angular distributions are compared with the results of MS$X\alpha$ calculations, and it is shown that the calculations and the experimental results agree in the main features. The occurrence of the 1π photoemission resonance is explained by an interaction of the outgoing electron with the adsorbed CO molecule and the nearby Pt atoms of the Pt(111) surface.

DOI: 10.1103/PhysRevB.83.125435 PACS number(s): 79.60.Dp, 33.60.+q, 42.65.Ky

I. INTRODUCTION

Carbon monoxide molecules adsorbed on noble- and transition-metal surfaces are well known and widely understood model systems for the study of surface-adsorbate interactions. Many theoretical and experimental investigations in the past four decades have led to a detailed understanding of the structure, electronic properties, and binding conditions. These features are changing significantly when CO is bound to different transition and noble metals and even on different surfaces of the same metal.[1,2]

The chemical bond between the CO molecule and surfaces of transition metals is often described using the Blyholder model.[3] In this model the binding is described by donation and back donation of electron density between molecular orbitals and the metal band structure without hybridization between these orbitals. A small fraction of the electron density from the highest occupied molecular orbital (HOMO) of the CO molecule, which is the 5σ state of the free molecule, is transferred to metal states. This donation is partly compensated by minor back donation of electron density from metal bands to the lowest unoccupied molecular orbital (LUMO) of the CO molecule, namely, the $2\pi^*$ orbital. This reallocation of charge carriers leads to a weakening of the internal CO bond and to an energetic shift of the 5σ state to higher binding energies relative to the uninvolved 1π and 4σ levels.

The Blyholder model was very successful in describing many experimental results when CO molecules are bound to transition-metal surfaces. But it does not take into account that hybridization between CO molecular orbitals and the metal band structure takes place and that new electronic states are formed.[4–6] Föhlisch *et al.* observed new electronic states induced by the CO-surface chemical bond using x-ray emission spectroscopy (XES) on Ni and Cu surfaces.[7,8] For noble- and transition-metal surfaces the adsorption-induced states often overlap with the metal d valence band.[2] Their signature is therefore often obscured by bulk substrate states. In combination with density functional theory (DFT) calculations they conclude, in contrast to the Blyholder model, that the π system formed between the molecular orbitals of π symmetry and metal d bands is stabilizing the surface adsorbate bond, whereas the σ interaction is destabilizing. In this picture, strong mixing between the 1π state and substrate states occur.

Depending on the substrate material and surface structure CO molecules may adsorb on several adsorption sites and in different orientations. On the Pt(111) surface the CO molecule is oriented perpendicular to the sample surface with the C atom pointing toward the surface.[9] On Pt(110), in contrast, the molecule is tilted against the surface normal by $\sim 26^\circ$.[10] On the Pt(111) surface at low coverages and low temperatures two stable adsorption sites have been observed. At low coverages the on-top position is energetically preferred. With increasing coverage also twofold coordinated bridge positions are occupied. When a coverage of 0.5 monolayers is reached, a $c(4 \times 2)$-2CO overlayer can be formed. In this case the top and bridge sites are equally populated. Also threefold hollow positions provide CO binding at higher temperatures and coverages.[11]

Although a deep understanding of the nature of the CO-metal chemical bond has been gained, there are still discussions about several questions that are left open. One of these open questions is the occurrence of a broad resonance in the photoelectron cross section of the $1\pi^{-1}$ state of CO at an photon energy of approximately $h\nu = 33$ eV on Pt(111).[12] This resonance has not been observed in gas-phase CO nor after adsorption on other transition-metal surfaces. Therefore we assume that this resonance is caused by characteristic properties of the Pt(111) surface interacting with the CO molecule. The photoelectron cross sections of the $4\sigma^{-1}$ and $5\sigma^{-1}$ states show broad features in the same energy range that can be attributed to $6\sigma^*$ shape resonances.[13,14] Such shape resonances have been observed for the CO molecule on several substrates[15,16] and also in the gas phase,[17,18] but, to the best of our knowledge, have never been observed for orbitals with π symmetry. Because the symmetry of the states involved plays a major role for photoemission cross sections due to selection rules, an investigation of the symmetry of the $1\pi^{-1}$ photoemission cross section at different photon energies across the resonance may lead to a deeper insight into the origin of this resonance and the processes involved.

Angle-resolved photoemission utilizing photon energies in the UV (ARUPS) is a common tool for symmetry

investigations of molecular orbitals if these molecules are fixed in space.[19] Therefore we have performed ARUPS measurements at different photon energies across the $1\pi^{-1}$ resonance to monitor the changes in the photoelectron angular distributions. High-order harmonics (HH) of intense ultrashort laser pulses are a photon source providing tunable radiation in the range from $h\nu = 20$ eV up to 110 eV, applicable in photoelectron spectroscopy experiments. In this work photon energies from $h\nu = 23$ to 52 eV generated in argon are used covering the resonances of the $4\sigma^{-1}$, $5\sigma^{-1}$, and $1\pi^{-1}$ states of CO adsorbed on Pt(111).

Additionally, we have calculated $OCPt_n$ clusters modeling the bond between CO molecules and the platinum surface. Calculations based on the electron density functional in various sophistications can yield electron binding energies with high precision. In several publications Ohno *et al.* calculated valence photoemission spectra for COPt and $COPt_2$ clusters using an *ab initio* Green's function method.[20,21] They showed that the quasiparticle picture breaks down for PtCO.[21] These calculations, however, do not easily yield photoelectron angular distributions. We therefore performed cluster calculations using quantum chemical methods, which directly yield the outgoing electron wave function. As a first step multiple electron scattering using a local exchange potential (MS$X\alpha$) are employed. Angle-resolved photoelectron cross sections of the different electronic states involved have been obtained at various photon energies and are compared to the experimental observations.

II. EXPERIMENT

High harmonic generation (HHG) of femtosecond visible laser pulses in noble gases such as argon, neon, and helium provides stepwise tunable extreme ultraviolet (XUV) pulses with femtosecond duration.[22,23] Laser intensities on the order of 10^{13}–10^{14} W/cm^2 are required to generate HH in noble gases. In the present experiment a mode-locked and cavity-dumped Ti:sapphire laser oscillator and a cryogenically cooled Ti:sapphire multipass amplifier are used. The oscillator emits pulses with energies of up to 30 nJ at repetition rates up to 400 kHz. These pulses are stretched by material dispersion, amplified, and recompressed in a prism compressor. At a central wavelength of 790 nm, pulse energies of more than 1 mJ with sub-30 fs [full width at half maximum (FWHM)] duration are generated. The amplifier repetition rate can be chosen up to 10 kHz without losing pulse energy. A detailed description of the laser system has been given previously.[24]

The experimental setup is shown in Fig. 1. The femtosecond laser pulses are focused into a gas target of ~1 mm length at a pressure of ~200 mbar, similar to the setup of Spielmann *et al.*[25] In the present experiments argon is employed as the nonlinear medium because it is the most efficient target for XUV photon energies between $h\nu = 20$ and 50 eV. Differential pumping stages evacuate the beam path to the grating chamber. A 100-nm-thick Al foil that is nearly transparent for photon energies between $h\nu = 20$ and 70 eV is inserted into the beam to block the fundamental light and additionally to block residual gas flow from the generation process to the sample chamber. The pressure within the grating chamber thus remains at 10^{-9} mbar. Because all odd harmonic orders are generated simultaneously, a toroidal grating is used to separate a single harmonic and to focus the XUV radiation onto the sample surface. Therefore the generation volume is used as an equivalent entrance slit, and the radiation is focused on an exit slit placed in front of the sample surface. The desired photon energy can be simply selected by turning the grating. Depending on the conversion efficiency of the selected harmonic order, the intensity of the HH at the sample position has to be significantly reduced to avoid space-charge effects.

The μ-metal ultrahigh vacuum (UHV) chamber with a base pressure of 10^{-10} mbar is equipped with ultraviolet

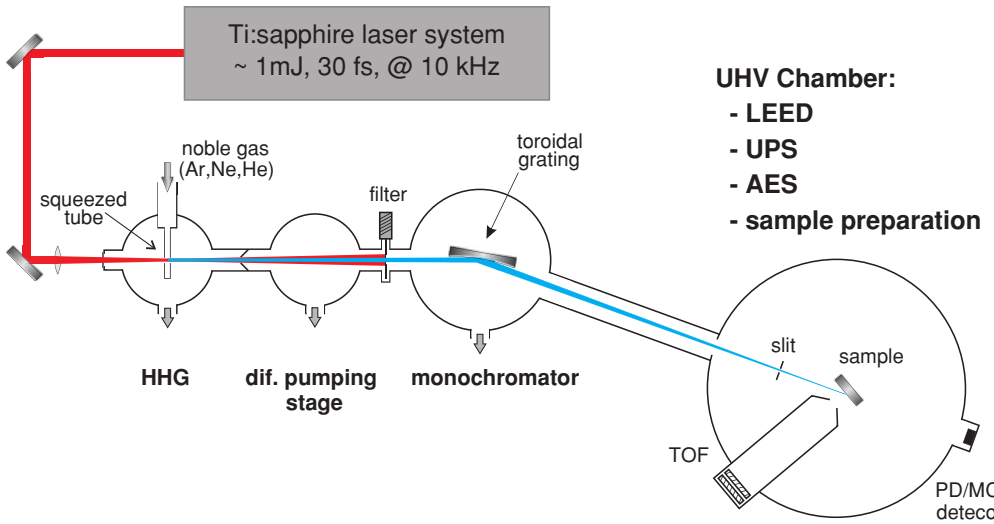

FIG. 1. (Color online) Schematic of the setup used in the experiments. The HH are generated by focusing the intense ultrashort pulses of a Ti:sapphire laser into rare gases such as Ar, Ne, or He. A differential pumping stage reduces the gas flow from the generation process to the surface. Thin metal foils can be used to block the fundamental beam. A toroidal grating is used to simultaneously separate the harmonic orders and to image the XUV pulses onto the sample surface. The generated photoelectrons are detected by a TOF spectrometer. Angle-resolved measurements can be performed by turning the sample in front of the spectrometer.

photoelectron spectroscopy (UPS) using a He discharge lamp and a dispersive electron spectrometer, Auger electron spectroscopy (AES), low-energy electron diffraction (LEED), and sample preparation tools. The Pt(111) single crystal is cleaned by cycles of Ar^+-ion bombardment with a kinetic energy of 1.5 keV at 700 K, oxidation also at 700 K, and annealing at 1050 K. After the surface is cleaned and checked by LEED and UPS, the $c(4 \times 2)$-2CO layer is prepared by dosing the sample surface with 2 Langmuir (L) of CO at 270 K.[26] The successful preparation is again checked by LEED observing the typical 4×2 superlattice. During the measurements the crystal temperature is held below 150 K to stabilize a defined CO superstructure on the platinum surface.

The ultrashort XUV pulses generated in the HHG process allow to record the photoelectron spectra by a time-of-flight (TOF) electron spectrometer. A field-free drift tube with a length of 216 mm is followed by a microchannel plate (MCP) electron detector. The flight time of the photoemitted electrons is determined by a time-to-digital converter. A small fraction of the fundamental pulse is detected by a fast photodiode to set a starting trigger. A total energy resolution of ∼0.6 eV is achieved. The angular resolution is limited by the size of the MCP detector and its distance to the surface, which results in an acceptance angle of $\Delta\vartheta = \pm 2.5^\circ$.

The angle between the incident light and the TOF axis is 5° (see Fig. 1). Angle-resolved photoemission experiments are performed by turning the sample in front of the TOF electron spectrometer. Therefore it has to be considered that the angle between the surface normal and the incoming light changes when changing the detection angle. If the XUV radiation is polarized perpendicular to the optical plane ($\hat{s}$ polarized), the electric field vector is orientated within the surface plane and its orientation relative to the sample does not change during angle-resolved measurements. If the polarization is chosen to be parallel to the optical plane ($\hat{p}$ polarized) the orientation of the electric-field vector relative to the sample changes when the sample is turned. This change has to be taken into account when comparing our results to other experimental or numerical investigations.

III. CALCULATION METHODS

A. The CO adsorption positions

The Pt(111) surface shows a C_{6v} symmetry with three mirror planes. The CO molecule adsorbs with its axes perpendicular to the surface in the C-down orientation. It is supposed in literature that upon CO adsorption on Pt(111) to a first approximation the positions of the Pt atoms in the first and in other layers do not change. With these suppositions we can distinguish four possible local positions of the CO molecule on the surface:[27] the on-top position, the bridge position, and the two fcp and hcp hollow positions. Experimentally only the on-top and bridge positions have been observed at low coverages, as mentioned above. To model the on-top bound CO molecules we have evaluated OCPt ($C_{\infty v}$ symmetry) and $OCPt_7$ (C_{6v}) clusters.

B. Computational details

Calculations are performed using the continuum multiple-scattering method with an $X\alpha$ local-exchange potential, MS$X\alpha$ method, which is based on the early work of Slater,[28] Slater and Johnson,[29] and Dill and Dehmer.[30] In spite of its relative simplicity, this method has been applied successfully to the electronic structure calculations of atoms, molecules, and solids. The method is based on the partitioning of the three-dimensional space into three kind of regions. For an n-atomic molecule the first region consists of n spheres containing the atomic cores at their centers. These spheres may touch each other, as in earlier calculations of the photoionization of diatomic molecules,[18,31] or overlap as in more recent calculations for polyatomic molecules.[32,33] A larger sphere encloses the atomic spheres and divides the remaining space into an outer sphere region with spherical symmetry, and an inner sphere region with (in some cases) axial symmetry.

The atomic potentials inside the small spheres are calculated using a localized exchange potential (the so-called $X\alpha$ potential) expressed through the charge density by analogy with an infinite electron gas.[28] Then the total energy has the same form as in the Hartree-Fock method. In the region outside of the atomic spheres but inside the outer sphere the potential is constant. And finally, outside the large sphere the $X\alpha$ or the Coulomb potential was taken, whichever is stronger. Since the $X\alpha$ potential decreases exponentially with distance, the Coulomb potential will eventually prevail.

In our numerical calculations the alpha exchange parameters for C, O, and Pt atoms are taken from the tabulation of Schwarz[34] to be 0.759 28, 0.744 47, and 0.693 06, respectively. The C-O interatomic distance of 1.15 Å is taken from literature.[27] Atomic sphere radii, obtained using the Norman procedure,[35] are commonly reduced by an empirical factor, which in the present case is close to 0.88. The radii for the C, O, and Pt inside the outer sphere are taken in such a way that the atomic spheres are overlapping. For the region inside the outer sphere and between the atomic spheres, the atomic alpha's are averaged with the same weights used in determining the outer sphere center. For the OCPt clusters the radii have been chosen to be 0.850, 0.867, 1.444, and 2.656 Å for C, O, Pt, and the outer sphere, respectively. For the calculations on $OCPt_7$ clusters different radii with values of 0.849, 0.867, 1.332, and 4.114 Å for C, O, Pt, and the outer sphere, respectively, have been used.

Multiple-scattering $X\alpha$ calculations of a self-consistent ground-state CO molecular potential follow the procedure of Case, Cook, and Karplus.[36] A significant number of partial waves ($l_{\max} = 7$) for the outer sphere and for the C, O, and Pt atoms are used in the calculations. The continuum wave function is calculated using the converged transition-state potentials, adapted to the correct asymptotic form by a Latter tail,[37] however, with 1.6 electrons instead of 2.0 on the respective orbital. It has been shown that, using a fractional charge, calculated ionization potentials show significantly better agreement with experimental data.[38] This so-called half-electron approximation considers the photoionization process where an atom with, initially, two electrons in the respective orbital is ionized and an ion with one electron is left. This method is similar to the so-called transition-state

approximation successfully applied by Ohno *et al.*[20,21] for the calculation of different CO-metal clusters. A program, originally written by Davenport[39] to calculate the photoionization cross section, was used to calculate the photoelectron angular distributions. For each experimental detection angle from -20° to $+90^\circ$ the angle between the light polarization and the CO axis is determined. With this information the full photoelectron angular distribution is calculated for each experimental detection angle in steps of 5°. The intensity in the direction of photoelectron detection is determined and displayed as a function of the detection angle. In order to enhance the possibilities of the program, some optimization of the code was done, especially in the input and output parts.

Different to the earlier MS$X\alpha$ calculations[31] where the CO potential was constructed with nonoverlapping atomic spheres, we used the overlapping spheres,[40,41] which evidently is a better approach for a molecular potential. It was shown recently[42] that a such modification, together with the optimized choice of the parameters, greatly improves the results for the CO molecule. As a result, the MS$X\alpha$ angular distributions are even in a better agreement with the experiment than the results of the more straightforward relaxed-core Hartree-Fock (RCHF) approximation. Similar MS$X\alpha$ calculations on a number of fluoroethylene molecules[43] and some other polyatomic molecules[32,33] also demonstrate the high reliability of the approach.

IV. RESULTS AND ANALYSIS

1. Resonances in the photoemission cross section

In gas-phase UV photoemission spectra of CO, three typical signals are observed which are assigned to emission from the $4\sigma^{-1}$, $1\pi^{-1}$, and the $5\sigma^{-1}$ state at binding energies of $E_{4\sigma} = -19.68$ eV, $E_{1\pi} = -16.53$ eV, and $E_{5\sigma} = -14.01$ eV, respectively.[44] When the CO molecule is bound to a transition-metal surface such as Pt(111), only two distinct structures appear at energies of approximately $E_{B1} = -12.5$ eV and $E_{B2} = -9.5$ eV relative to the Fermi level. The structure at $E_{B1} = -12.5$ eV is associated with the $4\sigma^{-1}$ state. At $E_{B2} = -9.5$ eV the $5\sigma^{-1}$ state and the $1\pi^{-1}$ state of the CO molecule are overlapping.[45] On platinum surfaces the separation between the $5\sigma^{-1}$ and the $1\pi^{-1}$ signal is $\sim$1 eV,[10] large compared to other transition metals. Therefore it is possible to separate this feature into contributions from the 5σ and 1π level.

Photoelectron spectra of the clean and CO-covered surface irradiated with a photon energy of $h\nu = 32.8$ eV are shown in Fig. 2. The upper spectrum in Fig. 2 shows emission from a clean Pt(111) surface. A work function of $\Phi_{\mathrm{Pt}} = (5.93 \pm 0.3)$ eV has been estimated. The two structures at binding energies of -2 and -4.5 eV below the Fermi level are caused by platinum d-band transitions.[9] Additional resonances in the photoelectron background appear at -10 and -14.5 eV that are attributed to final-state resonances of the Pt(111) surface,[46] and are discussed later.

The spectra of the CO-covered platinum surface are shown for $\hat{p}$- and $\hat{s}$-polarized radiation in the middle and lower trace of Fig. 2, respectively. In this case a work function of

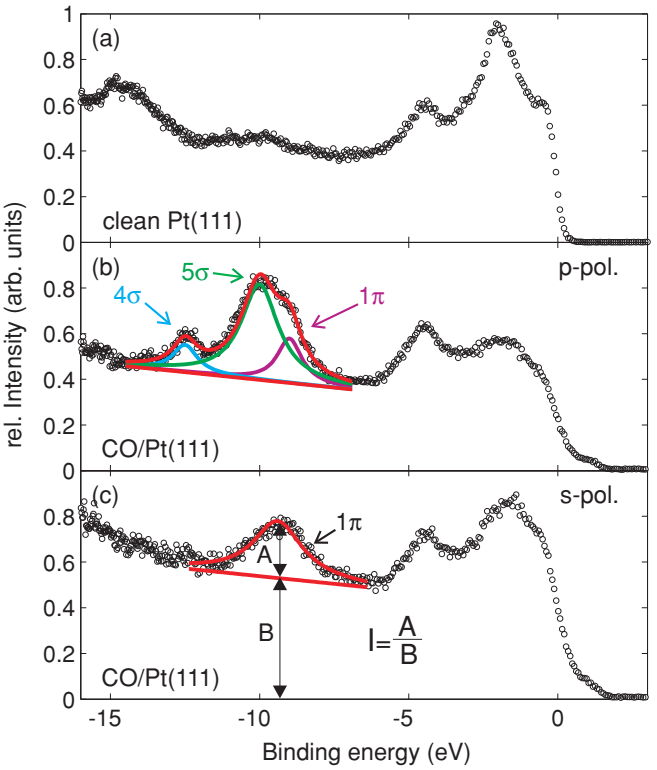

FIG. 2. (Color online) Photoelectron spectra taken with a photon energy of $h\nu = 32.8$ eV. The energetic positions and the relative amplitude of the individual structures of the $1\pi^{-1}$, $4\sigma^{-1}$, and $5\sigma^{-1}$ states are fitted by Lorentzian profiles. The relative photoelectron cross section is obtained by normalizing the amplitude of the structures to the background of scattered photoelectrons.

$\Phi_{\mathrm{CO/Pt}} = (6.0 \pm 0.3)$ eV has been measured. A decrease in intensity of the platinum d band next to the Fermi level upon CO adsorption is well known from synchrotron experiments. It is caused by donation of electrons to the CO molecule.[47] Besides the suppression of the Pt d band, additional structures appear that are attributed to the adsorbed CO molecules. For $\hat{s}$ polarization one CO-induced structure at a binding energy of $E - E_F = -9.0$ eV is assigned to the $1\pi^{-1}$ state. In $\hat{p}$ polarization two separated structures are visible, as mentioned above. A multiple peak fitting routine is used to retrieve the energetic positions and relative intensities of the individual overlapping structures of the $1\pi^{-1}$, $4\sigma^{-1}$, and $5\sigma^{-1}$ states. Applying a Lorentzian shape multiple fit and considering the scattered photoelectron background (see Fig. 2), the broad structure at $E - E_F = -9.5$ eV is separated into the contributions from the $1\pi^{-1}$ state at a binding energy of $E - E_F = -9.0$ eV and the $5\sigma^{-1}$ state at $E - E_F = -10.0$ eV. The $4\sigma^{-1}$ state is located at $E - E_F = -12.5$ eV. Taking into account the work function of our sample, our measurements can be compared easily to numerical calculations of the valence photoemission spectra by Ohno *et al.*[20,21] The energies of the main contributions to the photoemission from the $1\pi^{-1}$, $4\sigma^{-1}$, and $5\sigma^{-1}$ states have been calculated to be $E - E_F = -8.98$ eV, $E - E_F = -13.13$ eV, and $E - E_F = -9.48$ eV, respectively.[21] These results are in excellent agreement with our experimental data.

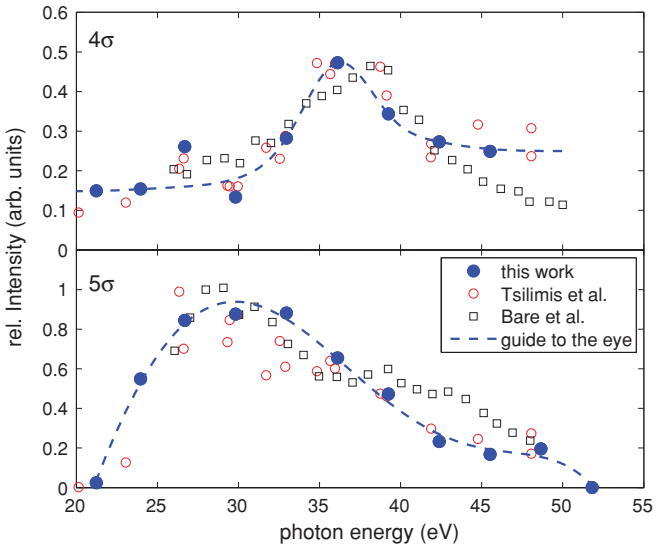

FIG. 3. (Color online) Relative photoemission cross section of the $4\sigma^{-1}$ and $5\sigma^{-1}$ states for different photon energies and $\hat{p}$-polarized light. The well-known shape resonances appear at photon energies of $h\nu = 36$ eV for the $4\sigma^{-1}$ state and $h\nu = 30$ eV for the $5\sigma^{-1}$ state. The data of Tsilimis *et al.* (Ref. 12) (red circles) and Bare *et al.* (Ref. 10) (black squares) show good agreement with the present data.

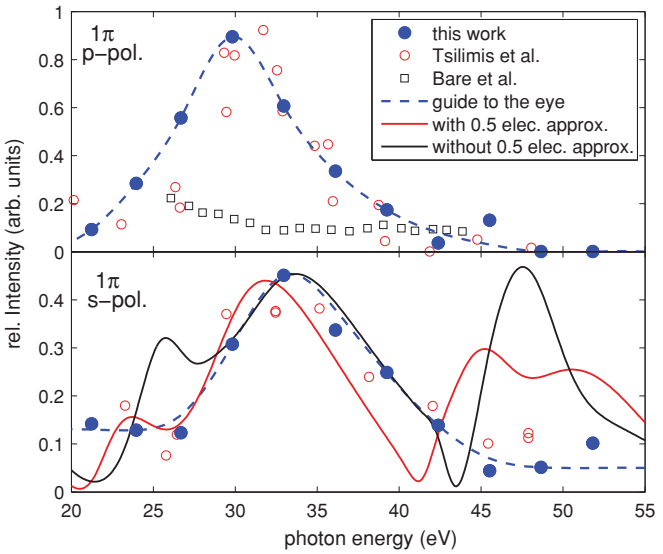

FIG. 4. (Color online) Relative photoemission cross section of the $1\pi^{-1}$ state at different photon energies. Distinct resonances have been observed at photon energies of $h\nu = 29.6$ and 33 eV for $\hat{p}$- and $\hat{s}$-polarized light, respectively. The data of Tsilimis *et al.* (Ref. 12) and Bare *et al.* (Ref. 10) [measured on Pt(110) surface] are added as red dots and black squares for comparison. No resonance has been observed on the Pt(110) surface.

The relative photoelectron cross sections are estimated with an approach similar to that established by Rieger *et al.*[15] After fitting the individual spectral features by Lorentzian curves their amplitude is normalized to the photoelectron background. This procedure is beneficial because no information about the photon flux and the detector characteristic are required.

The photoelectron emission cross sections of the σ orbitals as a function of the applied photon energy are shown in Fig. 3. Both structures show the well-known σ^* shape resonances at photon energies of $h\nu = 36$ and 30 eV for the $4\sigma^{-1}$ and $5\sigma^{-1}$ states, respectively. These resonances have been observed on several surfaces and in gas-phase experiments,[17] and these energetic positions fit well to literature values.[12,15] In Fig. 3 the data of Tsilimis *et al.*[12] (red circles) for CO/Pt(111) and of Bare *et al.*[10] (black squares) for CO/Pt(110) have been plotted as well, which show good agreement, although Bare *et al.* have measured on the Pt(110) surface. The occurrence of such shape resonances can be explained either by temporarily trapping of the excited electron in the potential barrier of the molecule[14,48] or by electron excitation to unoccupied and antibonding molecular levels above the ionization threshold.[13] In both shape resonances observed in this work, the $6\sigma^*$ orbital of the CO molecule is involved.

Although transitions from initial states of π symmetry to final states of σ symmetry are allowed, by selection rules no such shape resonances have been observed for π states so far. Tsilimis *et al.*[12] found an additional resonance in the cross section of the $1\pi^{-1}$ structure which has neither been observed in the gas phase[17] nor on other surfaces.[10] Measured relative photoelectron cross sections of the 1π orbital are shown in Fig. 4 for $\hat{s}$ and $\hat{p}$ polarization. For $\hat{p}$ polarization a resonance at a photon energy of $h\nu = 29.6$ eV is observed on Pt(111). For $\hat{s}$ polarization the resonance is shifted to slightly higher photon energies of $h\nu = 33$ eV. Again previous data of Tsilimis[49] and Bare[10] are plotted for comparison. The data taken on the Pt(111) surface show good agreement, while the data from the Pt(110) surface do not show a resonance in the measured energy range. Stener and co-workers[50] calculated photoelectron cross sections for gas-phase CO using time-dependent DFT and taking autoionization processes into account. Indeed, they also found structures in the energy range of the measured $1\pi^{-1}$ resonance. Tsilimis and co-workers therefore suggested that an autoionization process might be responsible for the resonance. They suggested that a resonant excitation from the 3σ orbital located at a binding energy of approximately $E - E_F = -28.5$ eV (Ref. 51) to the unoccupied $2\pi^*$ state located 4.3 eV above the Fermi level,[52] followed by a recombination and an autoionization of the 1π state, could lead to the enhanced cross section. These structures have not been observed in photoelectron experiments in gas-phase CO.[17,53] For the isoelectronic N_2 molecule, however, such a resonance in the photoelectron cross section for the $1\pi^{-1}$ structure for gas-phase molecules has been observed both experimentally[53–55] and theoretically.[56,57]

At the measured maximum of the 4σ shape resonance at $h\nu = 36$ eV (Fig. 3) the electrons from the 4σ state, bound at $E_B = -12.5$ eV, are detected with a kinetic energy of approximately $E_{\mathrm{kin}} = 17.5$ eV. For the $1\pi^{-1}$ signal in $\hat{s}$ polarization the resulting kinetic energy is approximately $E_{\mathrm{kin}} = 18.0$ eV. Considering the measured work function of the CO-covered Pt surface of $E_{\mathrm{vac}} = (6.0 \pm 0.3)$ eV, the resulting final-state energies for the photoemission process are $E - E_F = 23.5$ and 24.0 eV , respectively. The energetic position of the $6\sigma^*$ orbital that is responsible for the occurrence of the shape resonances in the $4\sigma^{-1}$ and $5\sigma^{-1}$ photoemission cross section has been measured for CO molecules chemisorbed on Ni(100) by inverse photoemission (IPE) and XAS to be approximately

$E_{6\sigma} - E_F = 24$ eV,[58,59] fitting well to our measured values. For the $5\sigma^{-1}$ structure and the $1\pi^{-1}$ structure in $\hat{p}$-polarization lower values for the kinetic energy of approximately $E_{\rm kin} =$ 14.0 and 14.6 eV have been measured, respectively, resulting in final-state energies of $E_B = 20$ and 20.6 eV. The similar experimental results for the value of the final-state energy for the measured resonances suggests that the resonances of the σ and π states are caused by the same or similar final states.

Final-state resonances in the photoemission background on the Pt(111) surface have been observed, as mentioned above.[46] These resonances have been explained by electron scattering into high-lying unoccupied electronic states of the Pt(111) surface. We observed resonances at kinetic energies of $E_{\rm kin} = 17$, 12.5, and 9 eV. The coincidence between the kinetic energies for the $4\sigma^{-1}$ and $1\pi^{-1}$ $\hat{s}$-polarized resonance maximum and the final-state structure at $E_{\rm kin} = 17$ eV is remarkable. An interplay between the substrate unoccupied electronic states and the $6\sigma^*$ orbital of the CO molecule may cause the resonance measured on this particular surface. For the $5\sigma^{-1}$ and $1\pi^{-1}$ $\hat{p}$-polarized resonance maxima the kinetic energies may be linked to the $E_{\rm kin} = 12.5$ eV final-state resonance. The energetic position of final states on this particular surface and the coincidence with the $6\sigma^*$ orbital may also explain why such resonances in the 1π photoemission cross section have not been observed on other surfaces or in gas-phase measurements.

For gas-phase carbon monoxide it is known[18] that for $\hat{s}$ polarization, i.e., the light being polarized perpendicular to the CO molecular axis, there is no resonance in the photoemission cross section. In order to confirm this fact we have calculated the photoemission cross section for $\hat{s}$-polarized light for gas-phase CO molecules using an intermolecular distance of 1.15 Å, which corresponds to the on-top adsorbed $OCPt_n$ clusters.[27] Under these conditions the MS$X\alpha$ calculations do not show a resonance for the 1π state. However, this 1π resonance appears for the OCPt cluster and the other calculated $OCPt_n$ clusters. In the lower part of Fig. 4 the calculated photoemission cross section is presented, with (red line) and without (black line) the half-electron correction for the $OCPt_7$ cluster. Because only relative photoelectron emission cross sections have been measured in this work, the calculated cross sections in this paper are scaled to fit the measured values. Both curves show a broad resonance at approxiamtely $h\nu = 33$ eV, where the resonance has been observed in the experiment. The curve without the half-electron correction additionally shows a rather sharp and high peak near a photon energy of $h\nu = 48$ eV and a feature at approximately $h\nu = 25$ eV. When the half-electron correction is included, the broad feature at $h\nu = 33$ eV is still retained, but the sharp peak becomes much broader and less intense. The structure at low photon energies of $h\nu = 25$ eV vanishes. When the half-electron correction is applied, the photoemission cross section of the $OCPt_7$ cluster shows good agreement for $\hat{s}$-polarized light with both sets of experimental data.

Previously, this half-electron approximation was used for MS$X\alpha$ CO (Ref. 42) and OCS (Refs. 60 and 61) potentials and for the RCHF CO potential.[38] Using this half-electron approximation gave, in all cases, a better agreement with precise experimental angle-resolved data. It also yielded a correct position for the maximum of the σ^* shape resonances in the photoionization cross sections. In the MS$X\alpha$ method a one-step photoemission process is modeled with the complete one-electron wave function for the outgoing electron. This means that we do not need to include some additional autoionization processes to be responsible for the 1π resonance. Since for the free diatomic CO molecule a 1π resonance does not appear in the MS$X\alpha$ calculations, this means that the 1π resonance results from scattering of the outgoing electron wave on the O, C, and especially the Pt atomic centers. At least three atomic centers are needed for the 1π resonance to appear.

2. *ARUPS in $\hat{p}$ polarization*

We have performed angle-resolved photoelectron measurements at photon energies between $h\nu = 26$ and 42 eV. Figure 5 shows photoelectron spectra taken at $h\nu = 39$ eV for different detection angles. Zero degree corresponds to the direction of the surface normal and is therefore parallel to the molecular axis of CO adsorbed on Pt(111). The individual structures of the CO- and Pt-derived states are clearly discernible, and the relative change in intensity of these structures is remarkable. The individual spectra at a specific angle have been normalized to the photoelectron background. The structures located at binding energies at $E_B = -2$ and -4.5 eV show only weak dispersion as expected from metal d-band structures. The $5\sigma^{-1}/1\pi^{-1}$ structures show an increasing intensity with a detection angle reaching a maximum at $\sim 45^\circ$. Fitting these spectral features with two Lorenzians, as described above, the $5\sigma^{-1}$ and $1\pi^{-1}$ photoelectron emission intensities can be extracted. For the three CO induced structures these relative cross sections are plotted in Fig. 6 as a function of the emission angle. The photoemission out of the 1π state shows a weak emission normal to the surface, and an increasing cross section with increasing angle. The 4σ and 5σ states show broad maxima at $\sim 15^\circ$ and 37°, respectively. Hofmann *et al.*[62] used the He II line at $h\nu = 40.8$ eV to measure photoelectron angular distributions of the same CO overlayer on Pt(111). This radiation was unpolarized so that $\hat{s}$- and $\hat{p}$-polarized light

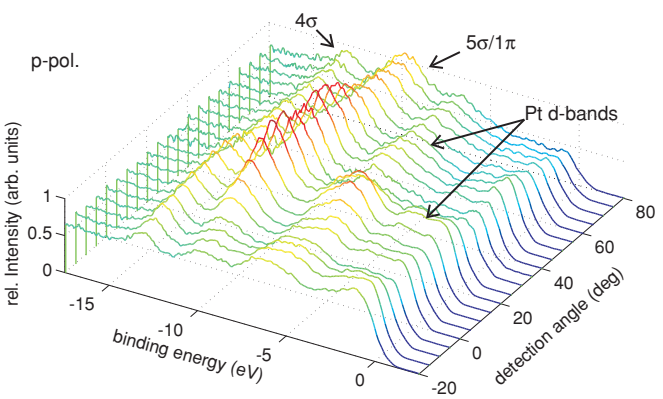

FIG. 5. (Color online) Photoelectron spectra taken at different detection angles with a photon energy of $h\nu = 39$ eV and p-polarized light. The CO induced structures at $E_B = -9.5$ and -12.5 eV display a significant change in intensity with detection angle. At positive angles the sample is turned toward the incident XUV light beam.

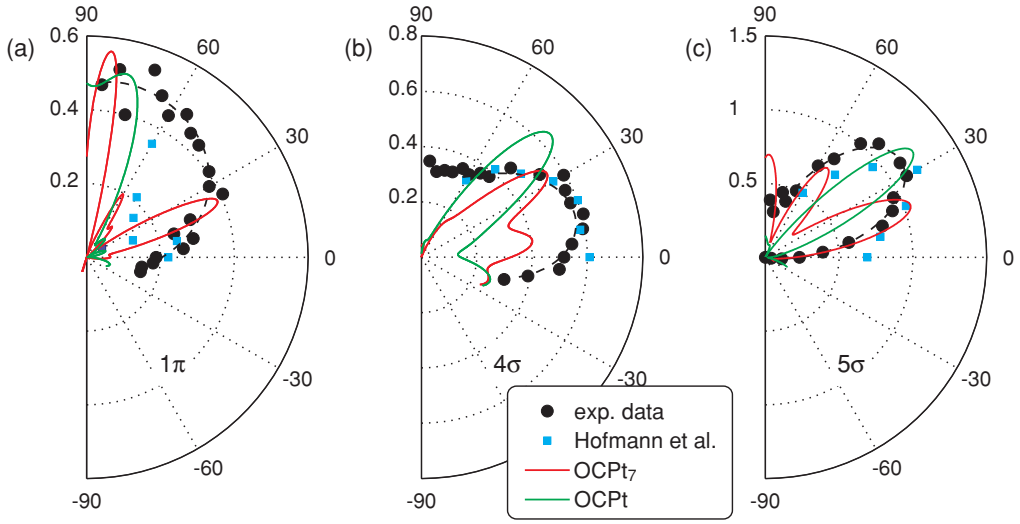

FIG. 6. (Color online) Relative photoemission cross section of the (a) $1\pi^{-1}$, (b) $4\sigma^{-1}$, and (c) $5\sigma^{-1}$ resonances as a function of the detection angle measured with a photon energy of $h\nu = 39$ eV and p-polarized light. Data of Hofmann *et al.* (Ref. 62) measured using unpolarized light at $h\nu = 40.8$ eV (He II) are plotted for comparison. See the text for more details.

were applied simultaneously. The angle of incidence was 45° relative to the surface normal. Their data are plotted as blue squares in Fig. 6.

The angular distributions of the $4\sigma^{-1}$ state agree very well in both experiments, although in the present case only $\hat{p}$-polarized light is applied, while Hofmann *et al.* used unpolarized light. However, the $\hat{s}$-polarized component should have no influence on the photoelectron distributions because the σ orbitals can only be observed in $\hat{p}$ polarization, as mentioned above. Also the shape of the angular distribution of the $5\sigma^{-1}$ state is similar in both experiments, but the maximum appears at slightly different angles. This may be caused by the fact that in the present experiments the sample has to be turned, thereby changing the angle between the molecular axis and the polarization vector, while it was fixed in the setup of Hofmann *et al.* The situation is completely different in the case of the $1\pi^{-1}$ state: Both experiments show considerably different results. At an angle of incidence of 45° the 1π orbital can be excited with either $\hat{s}$- or $\hat{p}$-polarized light and thus enabling photoemission processes with different symmetry and different photoelectron distributions when unpolarized light is applied.

Angle-resolved MS$X\alpha$ calculations have been performed at $h\nu = 39.1$ eV, for 1π, 4σ, and 5σ states for both OCPt and $OCPt_7$ clusters. The calculated relative photoemission cross sections for OCPt and $OCPt_7$ clusters are presented in Fig. 6 as full lines. The theoretical photoemission cross sections are significantly more structured than the rather smooth experimental curves, especially for the 1π state. The calculated relative photoemission cross section of the 1π state for the OCPt cluster shows a low cross section perpendicular to the surface ($\vartheta = 0°$ detection angle) and an increasing intensity toward higher angles. In the same figure the theoretical curve for the $OCPt_7$ cluster is presented. This photoelectron distribution (PED) also shows a low cross section normal to the surface, but a rather sharp maximum at $\vartheta = 25°$ is observed. The measured PED for the $1\pi^{-1}$ emission is not fitted well by these calculated angular distributions.

For the $4\sigma^{-1}$ emission the calculated PED of the OCPt cluster shows a minimum $\vartheta = 0°$ and a maximum at approximately $\vartheta = 45°$. For the $OCPt_7$ cluster maxima at approximately $\vartheta = 7°$ and $\vartheta = 35°$ appear. The measured PED is reproduced much better than for the $1\pi^{-1}$ emission and trends are reproduced, although there are notable differences. It has to be mentioned that the angular resolution of the experiment has not been taken into account in the calculated PEDs.

The calculated PED for the 5σ state and the OCPt cluster shows one rather sharp maximum at $\vartheta = 35°$. The positions of the experimental and calculated maxima coincide, but the experimental one is significantly broader. For the $OCPt_7$ cluster three maxima at $\vartheta = 20°$, $\vartheta = 55°$, and $\vartheta = 85°$ appear. This appearance of additional maxima in the calculations for $OCPt_7$ is a result of the electron wave dispersion on additional Pt atoms in $OCPt_7$, which can be noticed also for the 4σ and 1π peaks.

The experimental PEDs are significantly broader for both 1π and 4σ states than the 5σ distribution. For both states the calculated curves approximate the experimental distribution much worse than for the 5σ states. The large discrepancy for the 1π state may be associated with the fact that experimentally the intensity of the 1π state is only obtained after a deconvolution of the $5\sigma/1\pi$ resonances and the 1π state being the weaker shoulder. On the other hand, the relative maxima intensities in the three states reproduce the experimental data very well.

3. *ARUPS in $\hat{s}$ polarization*

For $\hat{s}$ polarization ARUPS measurements have been performed at six photon energies across the $1\pi^{-1}$ resonance at $h\nu = 26.6$, 29.7, 32.8, 36.0, 39.1, and 42.2 eV (see Fig. 7). All six distributions show the main intensity at angles from $\vartheta = -20°$ to $+20°$ and from $\vartheta = 60°$ to 85°. At approximately $\vartheta = 30°$ to $+40°$ a more or less pronounced minimum appears. At $h\nu = 32.8$ eV, near the maximum of the $1\pi^{-1}$

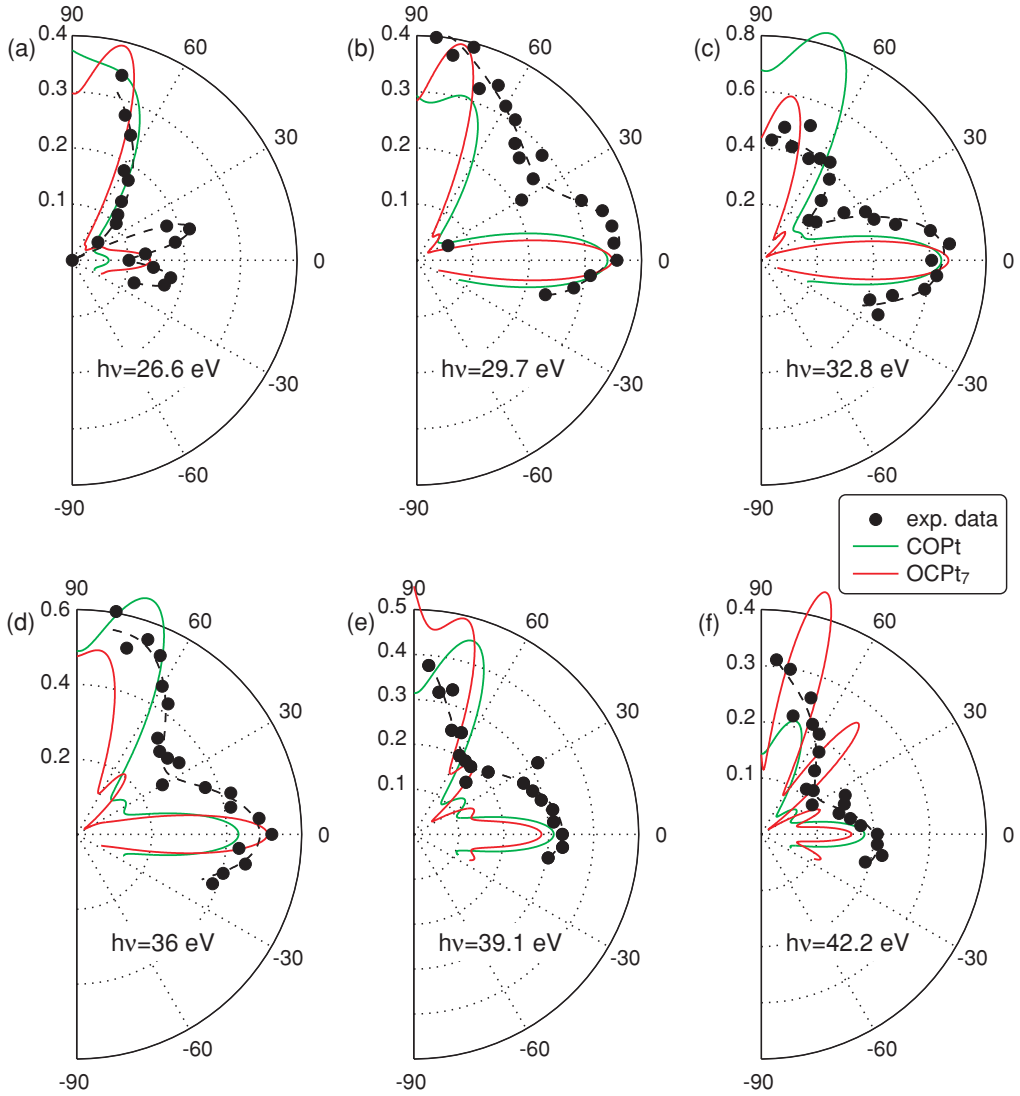

FIG. 7. (Color online) Photoelectron distributions for electrons emitted from the $1\pi^{-1}$ state of CO on Pt(111) measured with *s*-polarized light and at different photon energies: (a) 26.6 eV, (b) 29.7 eV, (c) 32.8 eV, (d) 36 eV, (e) 39.1 eV, (f) 42.2 eV. The photon energy is scanned over the resonance in the $1\pi^{-1}$ cross section to follow the evolution of the photoelectron distribution. The intensity scales are normalized to each other.

resonance, the intensity ratio of the two peaks maximizes with approximately 1.3:1 in favor of the normal ($\vartheta = 0^\circ$) to the oblique peak. In the spectral wings of the resonance the intensity of the normal emission peak is smaller than the oblique one.

The first photoelectron distribution has been taken at a photon energy of $h\nu = 26.6$ eV [Fig. 7(a)]. At this photon energy the signal of the $1\pi^{-1}$ state perpendicular to the surface is still small, because the resonance appears only at higher photon energies, in agreement with the expected gas-phase cross section, which is also small.[18] A large photoelectron cross section nearly parallel to the surface is visible ($\vartheta \sim 80^\circ$), beside two small features at $\pm 15^\circ$. The ratio between emission normal to the surface and emission nearly parallel to the surface is approximately 0.33:1.

When increasing the photon energy to $h\nu = 29.7$ eV, the photoelectron cross section normal to the surface increases significantly [Fig. 7(b)]. This photon energy has been chosen on the rising slope of the resonance. The two structures at $\vartheta = \pm 15^\circ$ disappear and one pronounced peak at $\vartheta = 0^\circ$ is formed. Again a minimum in the cross section at approximately $\vartheta = 30^\circ$–40° is visible, but it is less developed than in the other experimental curves in Fig. 7. The intensity ratio in this PED is approximately 0.89:1 for the normal to the oblique maximum.

When increasing the photon energy to the maximum of the resonance at $h\nu = 32.8$ eV [Fig. 7(c)] also the intensity in normal emission maximizes. The distinct structure normal to the surface dominates the angular distribution, while the oblique cross section has not changed significantly. The experimental intensity ratio of both peaks reaches a value of 1.30:1. When the photon energy is increased further the intensity in the normal direction decreases again [Figs. 7(d)–7(f)], following the cross-section measurement displayed in Fig. 4. The intensity ratio between normal

and perpendicular emission is also reduced to approximately 0.67:1 for a photon energy of $h\nu = 42.2$ eV.

The peak intensity ratio between the normal and the oblique peak is roughly following the shape of the resonance. The emission cross section in the normal direction, on the other hand, first increases and then decreases again when the photon energy is changed. One can conclude that the photoemission cross sections for the off-normal direction $\vartheta = 60^\circ$ and 85°, which are nearly perpendicular to the molecular axis, are much weaker influenced when the photon energy is scanned across the resonance than the normal emission one. The 1π shape resonance is therefore associated with photoemission in the direction normal to the surface only. This finding supports the above-mentioned assumption that the $1\pi^{-1}$ cross-section resonance is caused by Pt final states mixing with the $6\sigma^*$ CO molecular orbital because of the Pt final-state dispersion.

Earlier, Davenport calculated the photoelectron angular distribution for free CO molecules.[18] For $\hat{s}$-polarized excitation a large cross section perpendicular to the molecular axis and only a small cross section parallel to molecular axis were found. As mentioned above, in the present MS$X\alpha$ calculations we find a similar angular distribution for CO alone, with a low-intensity peak along the molecular axis and no 1π state resonance. MS$X\alpha$ calculations for OCPt and $OCPt_7$ clusters are constructed at all experimental photon energies across the 1π resonance. For the OCPt clusters the calculation yields for all photon energies two main peaks in the angular distribution, one along the surface normal and one at $\vartheta \sim 75^\circ$, with an angular spread of $\Delta\vartheta \sim 30^\circ$. These results are shown in Fig. 7 as a green line. This constitutes already a much better approximation to the experimental findings than the corresponding values calculated for the free CO molecule. The results for the $OCPt_7$ clusters are shown as red lines in Fig. 7 and show similar peaks at $\vartheta \sim 75^\circ$ and $\Delta\vartheta \sim 30^\circ$. The intensity ratios of the two peaks calculated for OCPt and $OCPt_7$ clusters fit well to the experimental data. The calculations for $h\nu = 26.6$ eV [Fig. 7(a)] show a small signal in the normal direction and a large photoelectron cross section in the oblique peak, but there are no structures at $\pm 15^\circ$. There are two possible explanations of such a difference. First, at this energy below the resonance these small structures appear as a result of the extraction of the 1π part from the overlapped $5\sigma/1\pi$ band. The second possible explanation is connected with a significant difference of our rather simple OCPt model clusters and the rather complex picture of real CO adsorption on a Pt(111) surface. The calculated PEDs for $h\nu = 29.7$ eV show a significant photoemission cross section in the normal direction, as expected for a photon energy in the rising slope of the resonance. For both clusters the peak ratio fits well to the experimental data. At the normal cross-section maximum at $h\nu = 32.8$ eV the peak intensity ratio for the $OCPt_7$ cluster fits well the experimentally observed distribution, while the OCPt calculation results in a too large cross section in the oblique peak. It should be kept in mind, however, that a model of a rigid linear OCPt molecule is a rather poor approximation of the real picture of an adsorbed CO molecule on the Pt(111) surface at a finite temperature of $\sim$150 K.

For a photon energy of $h\nu = 36$ eV, on the falling slope of the resonance, the peak intensity ratio for the both theoretical clusters fit well to the experimental findings, and the PED is roughly reproduced. For $h\nu = 39.1$ eV the oblique peak intensity is overestimated for both clusters. For $h\nu = 42.2$ eV the calculated PED for the OCPt cluster fits well to the experimental findings while the calculated $OCPt_7$ cross-section ratio again overestimates the oblique peak. Table I summarizes the intensity ratios between the normal and oblique structure for the experimental and numerical data for both clusters.

TABLE I. Summary of intensity ratios between emission normal to the surface and emission nearly parallel to the surface for the experimental data and the numerical data for OCPt and $PCPt_7$ clusters.

Photon energy	Experiment	OCPt	$OCPt_7$
26.6	0.33:1	0.17:1	0.35:1
29.7	0.89:1	1.16:1	0.85:1
32.8	1.30:1	1.03:1	1.08:1
36.0	0.91:1	0.73:1	1.04:1
39.1	0.82:1	0.67:1	0.56:1
42.2	0.67:1	0.82:1	0.40:1

The calculated PEDs are again notably more structured than the measured distributions. From the comparison presented here and some calculations for other $OCPt_n$ clusters, we can conclude that theoretical calculations and experimental data agree in the main features for both clusters that have been investigated. The differences in the calculated photoelectron distributions between OCPt and $OCPt_7$ clusters are small. Therefore, OCPt clusters are sufficient to describe the main effects discussed in this paper. This may be explained by a strong localization of the 1π orbital on the CO molecule and the first metal atom. This localization for the 1π state has been observed in DFT calculations for the on-top position on Ni and Cu surfaces by Föhlisch *et al.*,[7] and it is reasonable to expect a similar behavior on Pt surfaces. To the best of our knowledge, no shape resonances for states of π symmetry have so far been observed for diatomic molecules.

It has to be mentioned that the experimental angular resolution of $\Delta\vartheta = \pm 2.5^\circ$ has not been taken into account in the discussion so far. The increased angular spread in the experimental data compared to the calculated PEDs, especially in normal direction, can to some extent be explained by the finite resolution of the setup. Additional differences are connected with a rather simple $OCPt_n$ cluster model used, not taking into account the influence of CO molecules on other positions.

The agreement between calculated and measured photoelectron angular distributions across the resonance in $\hat{s}$ polarization shows that the model applied for the calculations is suitable to describe the photoemission process from the $1\pi^{-1}$ state. It is obvious that the photoelectron angular distributions in $\hat{p}$ polarization are not that well reproduced. Therefore, and because the maximum of the resonance in $\hat{p}$ polarization is found at other photon energies than the one in $\hat{s}$ polarization, additional processes may contribute to this resonance in $\hat{p}$ polarization.

V. SUMMARY

Angle-resolved ultraviolet photoelectron spectroscopy (ARUPS) based on high harmonic generation (HHG) of ultrashort laser pulses has been used to investigate the CO molecule adsorption on the Pt(111) surface in the photon energy range from $h\nu = 23$ to 52 eV. In this photon energy region photoemission resonances for 4σ, 5σ, and 1π states are found and compared with known experimental data. The relative photoemission cross section for these resonances as a function of detection angle is measured for $\hat{p}$-polarized light at a photon energy of $h\nu = 39.1$ eV. The photoelectron angular distributions for electrons emitted from the 1π state of CO on Pt(111) is measured with $\hat{s}$-polarized light across the resonance at six photon energies from $h\nu = 26.6$ to 42.2 eV. In all cases a significant photoemission yield in the normal direction is observed.

Additionally, MS$X\alpha$ calculations of the CO molecule and $OCPt_n$ clusters are carried out and compared with the experimental data. The MS$X\alpha$ method, extended to rather large clusters, is applied for studying different phenomena in the photoemission from adsorbed molecules. For such an application the majority of more sophisticated methods have not yet been extended. Our calculations, together with similar studies on the photoionization of polyatomic molecules by Powis and co-workers,[32,33] clearly demonstrate the ability of the MS$X\alpha$ method to be used for the description of rather delicate phenomena in photoionization of fixed-in-space molecules. From that one may conclude that it can be successfully applied for much larger objects, too.

The calculated 1π resonance curve for the $OCPt_7$ cluster potential with the half-electron approximation resembles to a certain extent the experimental data. This implies that the 1π resonance appears as a result of the scattering the outgoing electron wave on O, C, and especially Pt atomic centers. The resonance can be explained as a shape resonance. The coincidence of the kinetic energies measured for electrons scattered to energetically high-lying unoccupied states on the clean Pt(111) and the maximum of the shape resonances support this conclusion. It has to be kept in mind that unoccupied electronic states can be explained as an interference of scattered electrons from the atomic centers.

A careful analysis of the measured and calculated photoelectron distributions emitted from the 1π state measured with $\hat{s}$-polarized light shows that the calculations and experiment agree in the main features. A distinct change of the photoemission cross section in the normal direction occurs as expected for such a final-state effect. The fact that no resonance in the photoemission cross section of the 1π state has been observed on other surfaces nor in the gas phase suggests the importance of the final states on the Pt(111) surface for the photoemission cross section from the 1π state. Thus an interplay between the unoccupied states of the free CO molecule and the clean Pt(111) surface is responsible for the occurrence of this shape resonance of π symmetry. Additional autoionization processes as assumed by Tsilimis and co-workers[12] do not have to be taken into account to explain the experimental results.

ACKNOWLEDGMENT

A.V.G. acknowledges the hospitality of the Westfälische Wilhelms-Universität Münster and the financial support of the RFBR Grant No. 09-03-00781-A.

*haarth@uni-muenster.de

[1] J. A. Rodriguez and D. W. Goodman, Science **257**, 897 (1992).
[2] B. Hammer, Y. Morikawa, and J. K. Nørskov, Phys. Rev. Lett. **76**, 2141 (1996).
[3] G. Blyholder, J. Phys. Chem. **68**, 2772 (1964).
[4] A. Nilsson, N. Wassdahl, M. Weinelt, O. Karis, T. Wiell, P. Bennich, J. Hasselström, A. Föhlisch, J. Stöhr, and M. Samant, Appl. Phys. A **65**, 147 (1997).
[5] P. Hu, D. King, M. Lee, and M. Payne, Chem. Phys. Lett. **246**, 73 (1995).
[6] H. Aizawa and S. Tsuneyuki, Surf. Sci. **399**, L364 (1998).
[7] A. Föhlisch, M. Nyberg, P. Bennich, L. Triguero, J. Hasselström, O. Karis, L. Pettersson, and A. Nilsson, J. Chem. Phys. **112**, 1946 (2000).
[8] A. Föhlisch, M. Nyberg, J. Hasselström, O. Karis, L. G. M. Pettersson, and A. Nilsson, Phys. Rev. Lett. **85**, 3309 (2000).
[9] G. Apai, P. S. Wehner, R. S. Williams, J. Stöhr, and D. A. Shirley, Phys. Rev. Lett. **37**, 1497 (1976).
[10] S. Bare, K. Griffiths, P. Hofmann, D. King, G. Nyberg, and N. Richardson, Surf. Sci. **120**, 367 (1982).
[11] D. F. Ogletree, M. A. Van Hove, and G. A. Somorjai, Surf. Sci. **173**, 351 (1986).
[12] G. Tsilimis, J. Kutzner, and H. Zacharias, Appl. Phys. A **76**, 743 (2003).
[13] D. Loomba, S. Wallace, D. Dill, and J. L. Dehmer, J. Chem. Phys. **75**, 4546 (1981).
[14] J. L. Dehmer and D. Dill, Phys. Rev. Lett. **35**, 213 (1975).
[15] D. Rieger, R. Schnell, and W. Steinmann, Surf. Sci. **143**, 157 (1984).
[16] P. Budau and G. Raşeev, Phys. Rev. B **51**, 16993 (1995).
[17] E. Plummer, T. Gustafsson, W. Gudat, and D. Eastman, Phys. Rev. A **15**, 2339 (1977).
[18] J. W. Davenport, Phys. Rev. Lett. **36**, 945 (1976).
[19] S. D. Barrett, Surf. Sci. Rep. **14**, 271 (1992).
[20] M. Ohno and W. von Niessen, Phys. Rev. B **45**, 9382 (1992).
[21] M. Ohno and W. von Niessen, Surf. Sci. **269–270**, 258 (1992).
[22] T. Haarlammert and H. Zacharias, Curr. Opin. Solid State Mater. Sci. **13**, 13 (2009).
[23] A. Melzer, D. Kampa, J. Wang, and T. Fauster, Phys. Rev. B **80**, 205424 (2009).
[24] J. Hüve, T. Haarlammert, T. Steinbrück, J. Kutzner, G. Tsilimis, and H. Zacharias, Opt. Commun. **266**, 261 (2006).
[25] C. Spielmann, N. Burnett, S. Sartania, R. Koppitsch, M. Schnürer, C. Kan, M. Lenzner, P. Wobrauschek, and F. Krausz, Science **278**, 661 (1997).
[26] K. L. Kostov, P. Jakob, and D. Menzel, Surf. Sci. **377–379**, 802 (1997).
[27] M. Lynch and P. Hu, Surf. Sci. **458**, 1 (2000).
[28] J. C. Slater, *Statistical Exchange-Correlation in the Self-Consistent Field* (Academic, New York, 1972), Vol. 6, pp. 1–92.

[29]J. C. Slater and K. H. Johnson, Phys. Rev. B **5**, 844 (1972).
[30]D. Dill and J. L. Dehmer, J. Chem. Phys. **61**, 692 (1974).
[31]D. Dill, J. Siegel, and J. L. Dehmer, J. Chem. Phys. **65**, 3158 (1976).
[32]P. Downie and I. Powis, Phys. Rev. Lett. **82**, 2864 (1999).
[33]Y. Hikosaka, J. H. D. Eland, T. M. Watson, and I. Powis, J. Chem. Phys. **115**, 4593 (2001).
[34]K. Schwarz, Phys. Rev. B **5**, 2466 (1972).
[35]J. G. Norman Jr., J. Chem. Phys. **61**, 4630 (1974).
[36]D. A. Case, M. Cook, and M. Karplus, J. Chem. Phys. **73**, 3294 (1980).
[37]R. Latter, Phys. Rev. **99**, 510 (1955).
[38]N. A. Cherepkov, S. K. Semenov, A. V. Golovin, J. Adachi, and A. Yagishita, J. Phys. B **37**, 4803 (2004).
[39]J. W. Davenport, Ph.D. thesis, University of Pennsylvania, 1976.
[40]F. Herman, A. R. Williams, and K. H. Johnson, J. Chem. Phys. **61**, 3508 (1974).
[41]M. Cook and M. Karplus, J. Chem. Phys. **72**, 7 (1980).
[42]A. Golovin and N. Cherepkov, J. Phys. B **35**, 3191 (2002).
[43]A. Golovin and I. Powis (private communication).
[44]R. E. Huffman, J. C. Larrabee, and Y. Tanaka, J. Chem. Phys. **40**, 2261 (1964).
[45]A. Bradshaw, Surf. Sci. **80**, 215 (1979).
[46]G. Tsilimis, G. Fecher, J. Braun, J. Kutzner, and H. Zacharias, Appl. Phys. A **78**, 177 (2004).
[47]D. A. Shirley, J. Stöhr, P. S. Wehner, R. S. Williams, and G. Apai, Phys. Scr. **16**, 1402 (1977).
[48]J. L. Dehmer, J. Chem. Phys. **56**, 4496 (1972).
[49]G. Tsilimis, J. Kutzner, and H. Zacharias, Surf. Sci. **528**, 171 (2003).
[50]M. Stener, P. Decleva, I. Cacelli, R. Moccia, and R. Montuoro, Chem. Phys. **272**, 15 (2001).
[51]J. N. Miller, D. T. Ling, P. M. Stefan, D. L. Weissman, M. L. Shek, I. Lindau, and W. E. Spicer, Phys. Rev. B **24**, 1917 (1981).
[52]V. Dose, J. Rogozik, A. M. Bradshaw, and K. C. Prince, Surf. Sci. **179**, 90 (1987).
[53]A. Hamnett, W. Stoll, and C. E. Brion, J. Electron. Spectrosc. Relat. Phenom. **8**, 367 (1976).
[54]J. A. R. Samson, G. N. Haddad, and J. L. Gardner, J. Phys. B **10**, 1749 (1977).
[55]P. R. Woodruff and G. V. Marr, Proc. R. Soc. London, Ser. A **358**, 87 (1977).
[56]S. K. Semenov, N. A. Cherepkov, G. H. Fecher, and G. Schönhense, Phys. Rev. A **61**, 032704 (2000).
[57]M. Stener and P. Decleva, J. Chem. Phys. **112**, 10871 (2000).
[58]S. L. Hulbert, X. Pan, and P. D. Johnson, Phys. Rev. B **35**, 7710 (1987).
[59]O. Björneholm, A. Nilsson, E. O. F. Zdansky, A. Sandell, H. Tillborg, J. N. Andersen, and N. Mårtensson, Phys. Rev. B **47**, 2308 (1993).
[60]A. V. Golovin, J. Adachi, M. Motoki, S. Takahashi, and A. Yagishita, J. Phys. B **38**, L63 (2005).
[61]A. V. Golovin, J. Adachi, S. Motoki, M. Takahashi, and A. Yagishita, J. Phys. B **38**, 3755 (2005).
[62]P. Hofmann, S. Bare, N. Richardson, and D. King, Solid State Commun. **42**, 645 (1982).